PERGAMON

Deep-Sea Research I 49 (2002) 197–210

DEEP-SEA RESEARCH
PART I

www.elsevier.com/locate/dsr

Instruments and methods

A rapid birefringence method for measuring suspended $CaCO_3$ concentrations in seawater

Christopher K.H. Guay*, James K.B. Bishop

Earth Sciences Division, Lawrence Berkeley National Laboratory, One Cyclotron Road, Berkeley, CA 94720, USA

Received 31 August 2000; received in revised form 31 May 2001; accepted 17 August 2001

Abstract

The extreme birefringence of calcium carbonate ($CaCO_3$) relative to other major components of marine particulate matter provides a basis for making optical in situ measurements of particulate inorganic carbon (PIC) in seawater. This concept was tested with a benchtop spectrophotometer equipped with a 1- and 10-cm path length sample cell and modified with linear polarizers to measure the birefringence of suspended particles. Sample suspensions containing 3–100% $CaCO_3$ (by weight) were prepared from calcareous marine sediment material and varying amounts of non-birefringent diatomaceous earth. The samples ranged in total suspended material from 0.003 to 249 mg l^{-1} and PIC from 0.03 to 1820 μmol $CaCO_3$ l^{-1}. A positive relationship was observed between birefringence and PIC, with response falling off as the total particle concentration and the relative abundance of non-$CaCO_3$ particles in the sample increased. Sensitivity increased linearly with optical path length, and absolute detection limits of 0.2–0.4 and 0.04–0.08 μmol $CaCO_3$ l^{-1}, respectively, were determined for path lengths of 1- and 10-cm based on the intrinsic signal noise of the modified spectrophotometer. Conventional (i.e., non-polarized) transmittance measurements were used to correct the birefringence signal for the sensitivity loss due to interference from scattering and absorption. Without further modification, this spectrophotometer-based method can be used (with a 10-cm cell) to quantify PIC in most surface ocean waters—including those influenced by coccolithophore blooms. The spectrophotometer results define performance requirements and design parameters for an in situ instrument capable of operating over the oceanic range of PIC.

Keywords: Oceanography; Carbon cycle; Calcium carbonates; Optical properties; Analytical techniques; Instruments

1. Introduction

Particulate inorganic carbon (PIC) in seawater consists of biogenic particles of calcium carbonate ($CaCO_3$). PIC occurs as both calcite and aragonite polymorphs of $CaCO_3$ in the marine environment, ranging in concentration from <0.01 μmol $CaCO_3$ l^{-1} in deep ocean waters to >30 μmol $CaCO_3$ l^{-1} in open ocean surface waters during phytoplankton blooms (Balch et al., 1996b). Values up to 120 μmol $CaCO_3$ l^{-1}—the highest ever recorded—were observed during a bloom in Norwegian coastal waters (Berge, 1962). The fraction of total suspended material (TSM) comprised by PIC varies widely throughout the ocean and generally increases with depth because organic

*Corresponding author. Tel.: +1-510-486-5245; fax: +1-510-486-5686.

E-mail address: ckguay@lbl.gov (C.K.H. Guay).

0967-0637/01/$ - see front matter
PII: S0967-0637(01)00049-8

matter is remineralized faster than $CaCO_3$ as particles sink through the water column. At stations previously occupied in the north and equatorial Pacific and south Atlantic, PIC accounted for roughly 3–30% of TSM (by weight) in samples collected above 50 m and 10–40% in samples collected below 200 m (Bishop et al., 1978, 1998; Bishop, 1989).

The dominant fraction of PIC in the water column is derived from coccolithophores (unicellular phytoplankton of the class Prymnesiophyceae), which produce external calcite plates (coccoliths) that can subsequently become detached from the living cell. Secondary sources of PIC include shells of foraminifera (calcite) and pteropods (aragonite). Coccolithophores are widely distributed throughout the global oceans (except in the polar regions) and experience prolific blooms that cover areas up to $5 \times 10^5\,km^2$ (Balch et al., 1996a) and persist for weeks to months. Coccolithophore standing stocks become very large during these blooms (as many as $1.15 \times 10^8\,cells\,l^{-1}$ were observed in fjord and coastal waters of western Norway; Berge, 1962), and concentrations of detached coccoliths are often much higher (Holligan et al., 1993). Because of the high backscattering efficiency of PIC, coccolithophore blooms increase the albedo of the ambient seawater and thus decrease the transfer of solar energy to the surface ocean and the amount of light available to phytoplankton for photosynthesis (Tyrell et al., 1999). Perturbations to the local ecosystem resulting from coccolithophore blooms can alter the structure of the plankton community and propagate to higher levels of the marine food web (e.g., Macklin, 1999).

The formation of PIC at seawater pH follows the general reaction:

$$2\,HCO_3^-(aq) + Ca^{2+}(aq) \Leftrightarrow CaCO_3(s) + CO_2(aq) + H_2O(l). \quad (1)$$

From Eq. (1), it is evident that PIC formation results in a net reduction of total dissolved inorganic carbon species (CO_2, H_2CO_3, HCO_3^-, and CO_3^{2-}, collectively referred to as ΣCO_2) and contributes to the flux of sinking particles that transport carbon from the surface to deep ocean (i.e., the biological pump). But PIC formation also decreases alkalinity and increases pCO_2 in surface marine waters, thereby reducing the capacity of the ocean for taking up atmospheric CO_2. While it is clear that PIC plays an important role in marine carbon cycling, much remains unknown about the processes governing its formation, transport and remineralization (Bishop, 1989; Milliman et al., 1999).

Our understanding of PIC cycling has been severely limited by conventional ship-based sampling techniques—i.e., chemical analyses of particulate material filtered from seawater. This method of sampling cannot adequately assess the factors governing spatial and temporal variability of PIC in the oceans (e.g., a 20-fold difference in PIC in the upper water column was observed over a 6-week period between successive occupations of Ocean Station Papa in the subarctic Pacific; Fig. 1). Balch and Kilpatrick (1996) have developed a method for measuring PIC by analyzing differences in light scattering before and after acidification of seawater samples. Although this method allows samples to be collected at a much higher rate than previously possible, it is still limited to ship-based deployments. Satellite remote sensing techniques have been used to observe

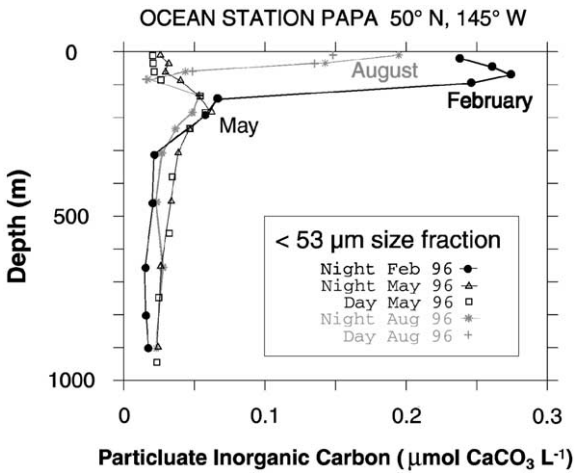

Fig. 1. Vertical profiles of PIC at Ocean Station Papa, in the subarctic Pacific, during three different occupations in 1996 (Bishop et al., 1998). Day/night cast data indicate significant diurnal PIC variability in surface waters.

the occurrence of coccolithophore blooms (e.g., Brown and Yoder, 1994), but these provide information only about the surface layer of the ocean and are hampered by cloud cover. Neither the onset nor the dissipation of a coccolithophore bloom has been observed (J. Aiken, personal communication, 1999).

We have been investigating a method for determining PIC concentrations in seawater based on the optical property of birefringence. Birefringence refers to the ability of a mineral crystal to split an incident beam of linearly polarized light into two beams of unequal velocities (corresponding to two different refractive indices of the crystal), which subsequently recombine to form a beam of light that is no longer linearly polarized (Rossi, 1957). The extreme birefringence of $CaCO_3$ makes it appear to light up when viewed through crossed polarizers—this characteristic mineralogical property of $CaCO_3$ is widely used as a means of identification (Fig. 2). Calcareous particles typically dominate the mineral fraction of marine particulate matter and are much more birefringent than other major classes of inorganic particles (Fig. 3). Although certain organic compounds may exhibit some degree of birefringence, polarized light micrographs of material filtered from seawater (e.g., Bishop et al., 1978, Fig. 23) suggest

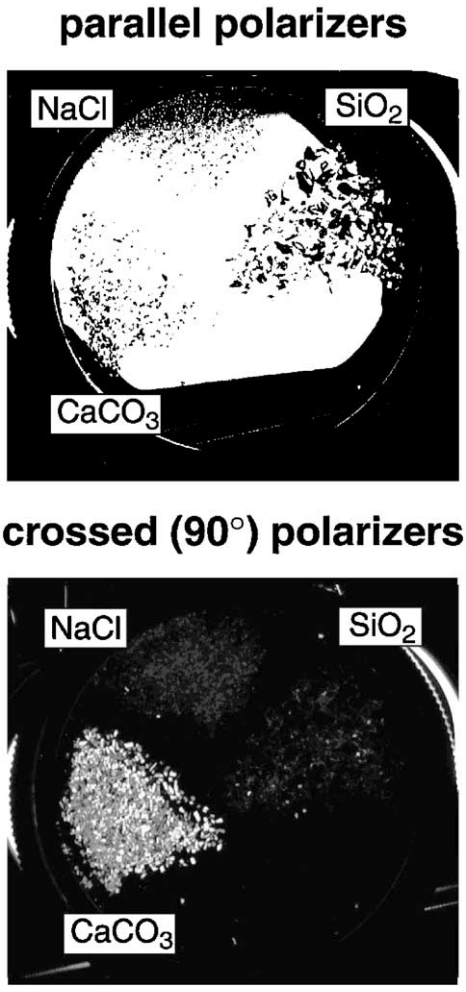

Fig. 2. The transmission of light through parallel and crossed polarizers by calcite and two non-birefringent minerals (halite and amorphous SiO_2).

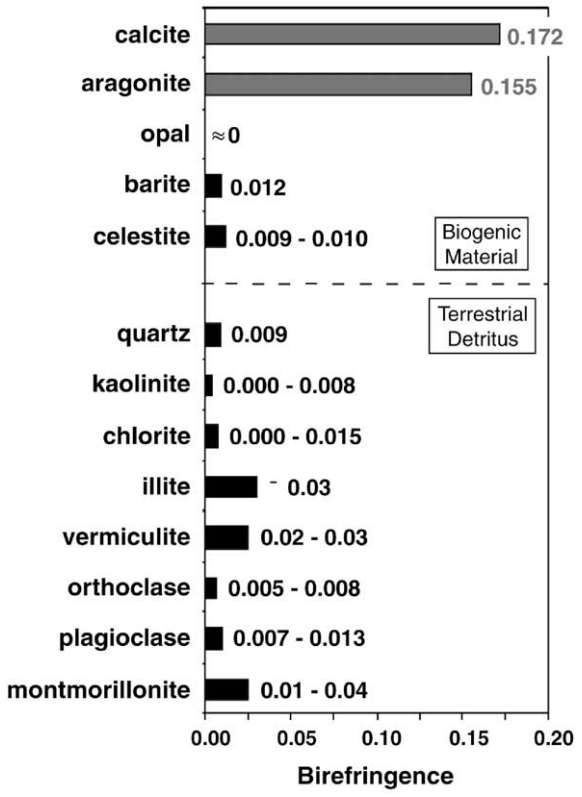

Fig. 3. Birefringence of major inorganic components of marine particulate matter (defined as the index of refraction in the direction of the mineral's long crystal axis minus the index of refraction in the direction of the mineral's short crystal axis). Data taken from Neese (1991).

that organic marine particles are weakly birefringent relative to $CaCO_3$ particles. We therefore expect PIC to be the dominant source of any birefringence signal obtained from seawater. Here we report results from initial laboratory experiments designed to test this idea and thus provide a basis for an in situ marine PIC sensor.

2. Methods

2.1. Preparation of suspensions

Suspensions were prepared from two sources of solid material: calcareous marine sediment collected from a site in the equatorial Pacific (0.95°N, 138.95°W, water depth = 4287 m); and commercially available powdered diatomaceous earth (i.e., a source of non-birefringent amorphous SiO_2). The calcareous sediment was rich in coccoliths but also contained a significant amount of calcite from larger foraminifera shell fragments. In order to isolate the fraction of smaller particles that would most readily remain in suspension, the following settling procedure was applied. Roughly 0.06 g of each material was added to a separate polyethylene bottle containing 120 ml of saturated $CaCO_3$ solution (used to minimize dissolution of $CaCO_3$). The bottles were placed in an ultrasonic bath for 10 min to break up any large aggregates of solid material and then shaken vigorously to suspend the particles in solution. The bottles were allowed to sit undisturbed for 30 min, at which point the upper 100 ml portion of each solution was collected for further use and the remainder discarded. Approximately 29% and 41% of the original amounts of calcareous sediment and diatomaceous earth, respectively, were recovered by this procedure.

After fractionation, a 10 ml aliquot of each suspension was passed through a 0.4 μm polycarbonate membrane filter. The filters were dried and weighed to determine TSM concentrations, then leached overnight in 2% HNO_3. The leachate was analyzed for Ca by inductively coupled plasma atomic emission spectroscopy to determine PIC concentrations for the suspensions as total acid-leachable Ca (Table 1). In the case of the diatomaceous earth suspension, it is likely that all of the Ca was not present as $CaCO_3$ and the reported PIC concentration should therefore be interpreted as an upper limit.

Table 1
Composition of the pure calcareous sediment and diatomaceous earth suspensions

	TSM ($mg\,l^{-1}$)	PIC ($\mu mol\ CaCO_3\,l^{-1}$)	% $CaCO_3$ (by weight)
Calcareous sediment	192	1820	95%
Diatomaceous earth	250	1.97	<1%

Particle size distributions were determined for the suspensions with a Coulter Multisizer II equipped with a 30 μm aperture. Particle diameters ranged from 0.74 μm (the smallest size detectable) to 9.1 μm in the calcareous sediment suspension and to 9.8 μm in the diatomaceous earth suspension. Particles with diameter <2 μm (i.e., typical coccolith size) dominated both suspensions.

2.2. Spectrophotometer analyses

Analyses were performed on an Amersham Pharmacia Biotech Ultrospec 3000 Pro benchtop spectrophotometer equipped with optical silica sample cells of both 1- and 10-cm path length. The spectrophotometer wavelength was set at 660 nm to match the red LED's commonly used in marine transmissometers (experiments conducted at different wavelengths yielded similar results). Transmittance (T) was measured and used to calculate absorbance (A) according to the standard relationship:

$$A = -\log_{10} T. \quad (2)$$

Note that in these experiments, "absorbance" is a measure of the amount of light attenuated from the incident beam due to both absorption and scattering by suspended particles.

To measure the birefringence of particles in suspension, the spectrophotometer was modified by installing a pair of Corning Polarcor linear polarizers (Fig. 4). Because light from the source lamp was already partially polarized by the grating monochrometer, it was possible to maximize the intensity of the fully polarized beam incident upon

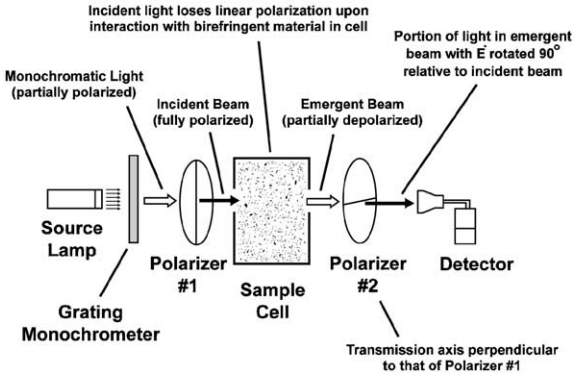

Fig. 4. Schematic diagram of spectrophotometer modified to detect birefringent material suspended in the sample cell.

the sample cell by rotating the polarizer between the source lamp and sample cell. The polarizer between the sample cell and the detector was rotated until the transmission of polarized light from the incident beam was minimized, i.e., the polarizers were crossed. Extinction ratios between 1.0×10^4 and 1.2×10^4 were typically achieved. To enable measurement of small signals above a near-zero background, the detector gain was set to approximately 275. The birefringence signal is reported as the ratio of the radiant power of the light reaching the detector (corrected for gain) to the radiant power of the light incident upon the front face of the sample cell.

3. 1-cm path length analyses

The pure calcareous sediment and diatomaceous earth suspensions were combined in different proportions and diluted with saturated $CaCO_3$ solution to give mixed suspensions containing 3%, 9%, 32%, 48%, and 64% $CaCO_3$ (by weight). Samples ranging in TSM from 1.3 to 250 mg l^{-1} and PIC from 12.1 to 1820 μmol $CaCO_3$ l^{-1} were prepared by serial dilutions of each of the pure and mixed suspensions. Aliquots of the suspensions (ranging in volume from 0.02 to 3 ml) were added to a 1-cm path length rectangular spectrophotometer cell and diluted to approximately 3 ml total volume with saturated $CaCO_3$ solution. The contents of the cell were agitated with a pipette before each analysis. Data were acquired digitally for 60 s at a rate of approximately 1 Hz and an average value was calculated.

Samples were prepared and analyzed separately for the conventional (i.e., non-polarized) transmittance and birefringence measurements. Each analytical run consisted of 17–31 samples and lasted 1–2 h. A reference cell containing particle-free, deionized water was run as a blank between groups of 5–10 samples. Data for the samples were blank-corrected by subtracting values linearly interpolated from the measured blanks.

4. 10-cm path length analyses

The procedure was identical to the one described above for the 1-cm path length analyses, with the following exceptions. Samples ranging in TSM from 0.003 to 30.8 mg l^{-1} and PIC from 0.03 to 67.8 μmol $CaCO_3$ l^{-1} were prepared by serial dilutions of the pure calcareous sediment and diatomaceous earth suspensions. Mixed suspensions containing 3%, 6%, 10%, 22%, 36%, 48% and 58% $CaCO_3$ (by weight) were prepared as individual samples immediately prior to analysis; these suspensions ranged in TSM from 0.9 to 30.6 mg l^{-1}, but all had PIC concentrations of $\sim$8.5 μmol $CaCO_3$ l^{-1}. Instead of saturated $CaCO_3$ solution, the diluent was surface seawater that had been passed through a 0.2 μm polycarbonate filter and brought up to pH 8.5 by adding small amounts of 0.15 N NaOH; this further reduced dissolution of $CaCO_3$ and significantly improved the stability of the suspensions over time. The diatomaceous earth material used in the suspensions was previously treated with acid and washed with deionized water to eliminate the possibility that it contained any $CaCO_3$. The samples were prepared in high-density polyethylene bottles and transferred by syringe to a 10-cm path length cylindrical spectrophotometer cell. Each analytical run consisted of 14–24 samples and lasted approximately 2 h. The filtered seawater diluent was run as a blank between groups of 1–8 samples.

5. Results

5.1. 1-cm path length analyses

Absorbance readings for the blanks were less than 0.001. Linear relationships were observed between absorbance and TSM for the serial dilutions of the pure calcareous sediment and diatomaceous earth suspensions (Fig. 5). The slope for the calcareous sediment data (2.50×10^{-3} l mg^{-1}) was more than twice as high as the slope for the diatomaceous earth data (1.18×10^{-3} l mg^{-1}; Table 2). Absorbance and TSM were linearly related for the serial dilutions of each of the suspensions containing mixtures of calcareous sediment and diatomaceous earth (Fig. 8). The slopes ranged from 1.12×10^{-3} to 2.00×10^{-3} l mg^{-1} (within the limits defined by the slopes for the pure calcareous sediment and diatomaceous earth suspensions) and increased in proportion to the $CaCO_3$ content of the suspensions.

The birefringence signal for the blanks ranged from 4.78×10^{-5} to 6.05×10^{-5} and drifted 1–3% over the course of an analytical run (Table 3). Over the PIC range of the samples (1.3–1820 μmol $CaCO_3$ l^{-1} μmol Ca l^{-1}), the blank-corrected birefringence signals ranged from to 6.48×10^{-6} to 6.88×10^{-4}—i.e., $<0.1\%$ of the radiant power of the incident light from the spectrophotometer source lamp. A positive relationship was observed between birefringence and PIC for the serial dilution of the pure calcareous sediment suspension (Fig. 6a). The response initially followed a linear trend (slope $= 5.37 \times 10^{-7}$ l μmol^{-1}; Table 2), falling off as PIC increased above 450 μmol $CaCO_3$ l^{-1}. Repeated analyses over the course of several months indicated that the slope of the birefringence response for different individual runs varied by $\pm 10\%$ or less.

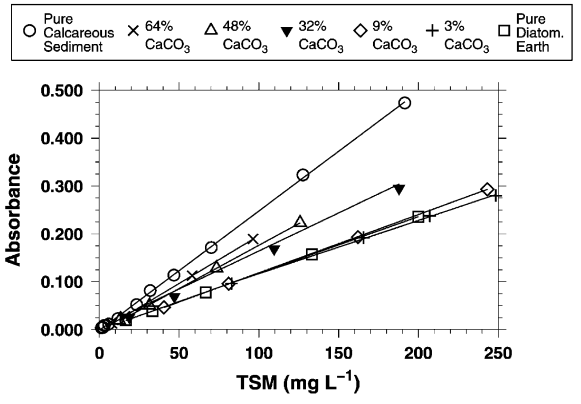

Fig. 5. Absorbance at 660 nm (1-cm path length) for serial dilutions of the pure and mixed suspensions containing calcareous sediment and diatomaceous earth. The solid lines indicate least-squares linear regressions of absorbance on TSM for each of the suspensions.

Birefringence and PIC were also positively correlated for the serial dilutions of the mixed suspensions with $CaCO_3$ content $\geqslant 9\%$ (Fig. 7a). As was observed for the pure calcareous sediment suspension, the response fell off as PIC increased. Sensitivity decreased as the relative proportion of $CaCO_3$ in the suspensions decreased, dropping approximately 2-fold between the pure calcareous sediment suspension and the 9% $CaCO_3$ suspension. No detectable signal was observed for the samples prepared from the 3% $CaCO_3$ suspension and the pure diatomaceous earth suspension.

The standard error over the 60 s acquisition period (4.32×10^{-8} to 6.42×10^{-8}) was roughly 0.1% of the birefringence signal for the blanks (Table 3). The minimum detectable birefringence signal (defined as three times the standard error of the blank) ranged from 1.30×10^{-7} to 1.93×10^{-7}. Based on the initial linear relationship between birefringence and PIC observed for the pure calcareous sediment (Fig. 6a, Table 2), the minimum detectable birefringence signal is produced by a PIC value of 0.2–0.4 μmol $CaCO_3$ l^{-1}. This represents the lowest detection limit possible for a 60 s data acquisition period and a 1-cm path length given the intrinsic signal noise of the modified spectrophotometer.

For the samples containing diatomaceous earth only, the standard error of the birefringence signal was roughly the same as that of the blanks. For the samples containing $CaCO_3$ (i.e., samples prepared from the pure calcareous sediment suspension and the mixed suspensions), the standard error was roughly 1–10 times that of the blanks. The standard error was generally higher at the upper end of the analytical range and dropped considerably as PIC decreased below 100–200 μmol

Table 2
Summary of least-squares linear regressions for the serial dilutions of the pure calcareous sediment and diatomaceous earth suspensions

	Calcareous sediment	Diatomaceous earth
1-cm path length		
Absorbance		
Number of samples	12	5
Slope ($l\,mg^{-1}$)	2.50×10^{-3}	1.18×10^{-3}
Standard error	1.76×10^{-5}	3.74×10^{-6}
Intercept	-1.75×10^{-3}	-6.33×10^{-4}
Standard error	1.26×10^{-3}	4.22×10^{-4}
Correlation coefficient (r^2)	0.999	1.000
Birefringence signal (initial linear response range—i.e., PIC $<450\,\mu mol\ CaCO_3\,l^{-1}$)		
Number of samples	9	—
Slope ($l\,\mu mol^{-1}$)	5.37×10^{-7}	—
Standard error	7.94×10^{-9}	—
Intercept	-9.03×10^{-7}	—
Standard error	1.58×10^{-6}	—
Correlation coefficient (r^2)	0.998	—
10-cm path length		
Absorbance		
Number of samples	11	12
Slope ($l\,mg^{-1}$)	2.50×10^{-2}	1.06×10^{-2}
Standard error	2.42×10^{-4}	9.02×10^{-5}
Intercept	1.30×10^{-3}	-5.15×10^{-5}
Standard error	9.02×10^{-5}	5.93×10^{-4}
Correlation coefficient (r^2)	0.999	0.999
Birefringence signal (initial linear response range—i.e., PIC $<20\,\mu mol\ CaCO_3\,l^{-1}$)		
Number of samples	20	—
Slope ($l\,\mu mol^{-1}$)	5.03×10^{-6}	—
Standard error	4.14×10^{-7}	—
Intercept	2.64×10^{-7}	—
Standard error	2.42×10^{-7}	—
Correlation coefficient (r^2)	0.999	—

$CaCO_3\,l^{-1}$ (Table 3). This indicates the greater variability inherent in a suspension of moving birefringent particles relative to particle-free solution.

The results from triplicate analyses of the 30.3, 303 and 1210 μmol $CaCO_3\,l^{-1}$ samples (Table 3) provide a measure of uncertainty due to both signal noise and procedural error (i.e., instrument drift, pipetting inaccuracy, etc.). For the 30.3 μmol $CaCO_3\,l^{-1}$ sample, the standard deviation of the triplicate analyses is of the same magnitude as the standard error of the average birefringence signal over the 60 s acquisition period for the individual analyses. The uncertainty in the measurement is therefore due primarily to signal noise at this concentration of PIC. For the 303 and 1210 μmol $CaCO_3\,l^{-1}$ samples, the standard deviation of the triplicate analyses is roughly an order of magnitude higher than the standard error of the average birefringence signal over the 60 s acquisition period for the individual analyses. This indicates that most of the uncertainty in the measurement at

Table 3
Blanks and replicate samples from a 1-cm path length birefringence run

PIC (μmol $CaCO_3 l^{-1}$)		Raw birefringence signal	Blank-corrected birefringence signal	Standard error for 60 s acquisition
Blank		5.062×10^{-5}	0	5.7×10^{-8}
		5.009×10^{-5}	0	4.4×10^{-8}
		4.975×10^{-5}	0	6.4×10^{-8}
		4.901×10^{-5}	0	5.6×10^{-8}
	Mean	4.987×10^{-5}	—	
	Std dev	6.729×10^{-7}	—	
	Rel std dev	1.35%	—	
30.3		6.65×10^{-5}	1.66×10^{-5}	2.2×10^{-7}
		6.58×10^{-5}	1.62×10^{-5}	7.9×10^{-8}
		6.53×10^{-5}	1.60×10^{-5}	1.5×10^{-7}
	Mean	6.59×10^{-5}	1.63×10^{-5}	
	Std dev	5.89×10^{-7}	2.80×10^{-7}	
	Rel std dev	0.89%	1.72%	
303		2.21×10^{-4}	1.71×10^{-4}	3.2×10^{-7}
		2.22×10^{-4}	1.72×10^{-4}	2.3×10^{-7}
		2.12×10^{-4}	1.62×10^{-4}	5.6×10^{-7}
	Mean	2.18×10^{-4}	1.69×10^{-4}	
	Std dev	5.68×10^{-6}	5.46×10^{-6}	
	Rel std dev	2.60%	3.24%	
1210		5.72×10^{-4}	5.22×10^{-4}	4.0×10^{-7}
		5.75×10^{-4}	5.25×10^{-4}	3.0×10^{-7}
		5.78×10^{-4}	5.29×10^{-4}	3.0×10^{-7}
	Mean	5.75×10^{-4}	5.25×10^{-4}	
	Std dev	3.08×10^{-6}	3.41×10^{-6}	
	Rel std dev	0.54%	0.65%	

higher concentrations of PIC is due to procedural error, with only a relatively small contribution from signal noise.

To verify that the birefringence signal was primarily due to the presence of $CaCO_3$ particles, undiluted pure calcareous sediment suspension was acidified and reanalyzed. Upon addition of HNO_3 to the sample cell, absorbance dropped from 0.474 to 0.013, in agreement with the 95% $CaCO_3$ content determined for the calcareous sediment material. Birefringence dropped from 6.42×10^{-4} to 2.77×10^{-6}, indicating that virtually all (99.6%) of the signal was due to $CaCO_3$. The small residual signal is consistent with the expected presence of clay minerals and other weakly birefringent material in the calcareous sediment.

5.2. 10-cm path length analyses

As was observed in the 1-cm path length analyses, absorbance and TSM were linearly related for the samples prepared from the pure calcareous sediment and diatomaceous earth suspensions. The slopes for the calcareous sediment data ($2.50 \times 10^{-2} l mg^{-1}$) and diatomaceous earth data ($1.06 \times 10^{-2} l mg^{-1}$) were 10 times higher than the slopes observed in the 1-cm path length analyses (Table 2). Absorbance measurements for the individual mixed suspensions fell between the lines fit to the data for the pure suspensions, decreasing proportionately as the $CaCO_3$ content of the suspensions decreased.

The birefringence signal for the blanks (2.34×10^{-5}–2.97×10^{-5}) was approximately two

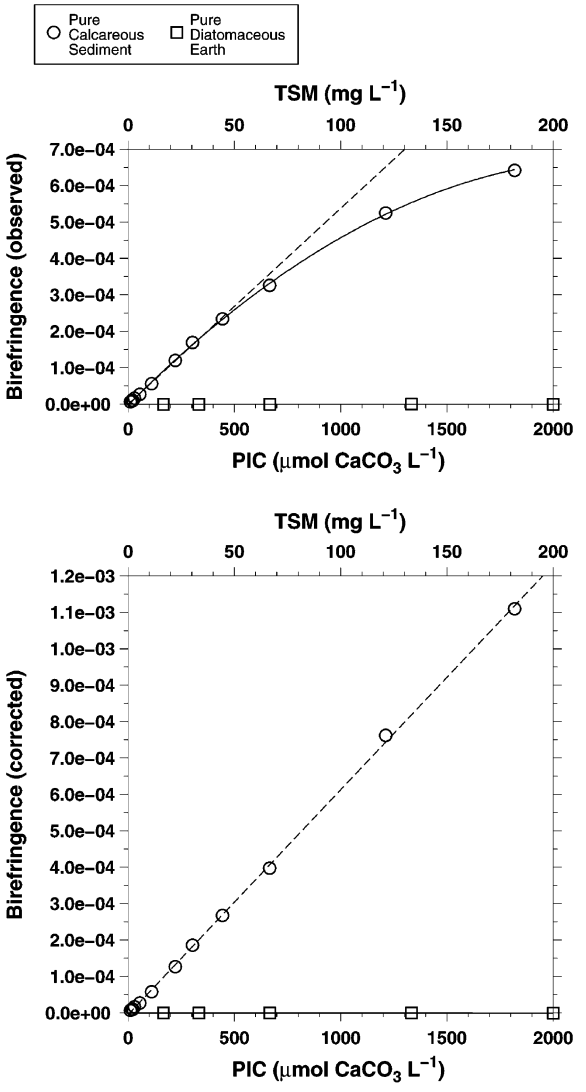

Fig. 6. (a) Observed and (b) corrected birefringence measured at 660 nm by the modified spectrophotometer (1-cm path length) for serial dilutions of the pure suspensions of calcareous sediment and diatomaceous earth. The TSM axis applies to both the calcareous sediment and diatomaceous earth data. The PIC axis applies to the calcareous sediment data only (i.e., PIC = 0 μmol $CaCO_3 l^{-1}$ for the pure diatomaceous earth samples). Error bars indicating 2σ precision for triplicate analyses of the 30.3, 303, and 1210 μmol $CaCO_3 l^{-1}$ samples are roughly the size of the data symbols or smaller. The dashed line on the upper graph indicates the least-squares linear regression of observed birefringence on PIC for the calcareous sediment samples with PIC <450 μmol $CaCO_3 l^{-1}$. The dashed line on the lower graph indicates the least-squares linear regression of corrected birefringence on PIC for all calcareous sediment samples.

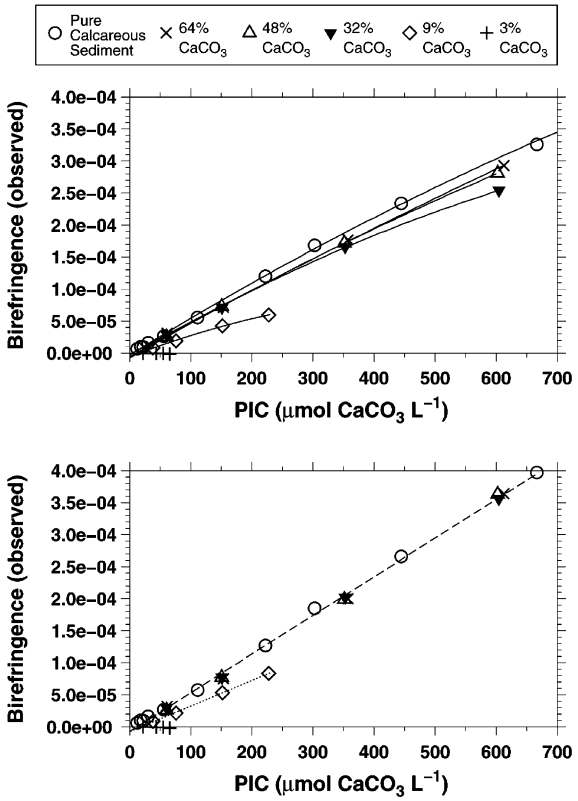

Fig. 7. (a) Observed and (b) corrected birefringence at 660 nm (1-cm path length) for serial dilutions of the pure calcareous sediment suspension and the mixed suspensions containing both calcareous sediment and diatomaceous earth. Two pure calcareous sediment samples with much higher PIC concentrations than the rest of the samples (1210 and 1820 μmol $CaCO_3 l^{-1}$) are not shown on these graphs. The dashed line on the lower graph indicates the least-squares linear regression of corrected birefringence on PIC for the combined data from the pure calcareous sediment suspension and the mixed suspensions with $CaCO_3$ content $\geqslant 32\%$. The dotted line on the lower graph indicates the least-squares linear regression for the 9% $CaCO_3$ suspension.

times lower than observed in the 1-cm path length analyses. Over the PIC range of the samples (0.03–67.8 μmol $CaCO_3 l^{-1}$), the blank-corrected birefringence signals ranged from 3.93×10^{-8} to 2.83×10^{-4}. For the samples prepared from the pure calcareous sediment suspension, the positive relationship between birefringence and PIC (Fig. 8a) was similar to the one observed with the 1-cm cell. The slope of the initial linear trend ($5.03 \times 10^{-6} l\,\mu mol^{-1}$) was roughly 10 times

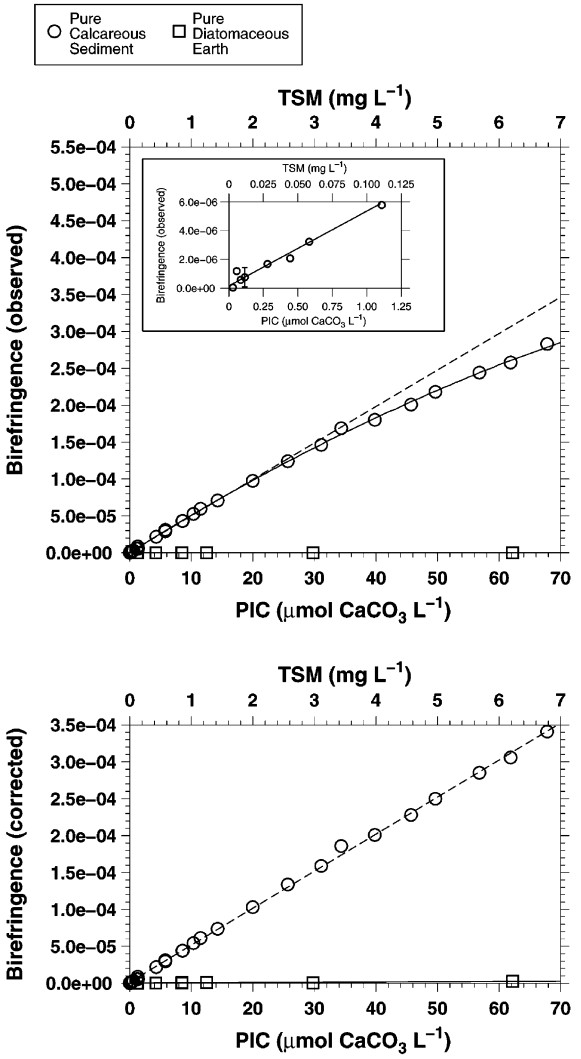

Fig. 8. (a) Observed and (b) corrected birefringence at 660 nm (10-cm path length) for serial dilutions of the pure suspensions of calcareous sediment and diatomaceous earth. The TSM axis applies to both the calcareous sediment and diatomaceous earth data. The PIC axis applies to the calcareous sediment data only (i.e., PIC = 0 μmol $CaCO_3$ l^{-1} for the pure diatomaceous earth samples). The dashed line on the upper graph indicates the least-squares linear regression of observed birefringence on PIC for the calcareous sediment samples with PIC <20 μmol $CaCO_3$ l^{-1}. The dashed line on the lower graph indicates the least-squares linear regression of corrected birefringence on PIC for all calcareous sediment samples. *Inset*: Blowup of low PIC region, including 2σ error bars based on triplicate analyses of the 0.12 μmol $CaCO_3$ l^{-1} sample (on the larger graphs, error bars for the 0.12, 10.4, 11.5, and 49.6 μmol $CaCO_3$ l^{-1} samples are roughly the size of the data symbols or smaller).

higher, and the response fell off as PIC increased above 20 μmol $CaCO_3$ l^{-1}. No detectable signal was observed for the samples prepared from the pure diatomaceous earth suspension. For the mixed suspensions, birefringence decreased as the $CaCO_3$ content of the suspensions decreased (Fig. 9a). At a PIC concentration of $\sim$8.5 μmol $CaCO_3$ l^{-1}, the birefringence signal dropped approximately 30% between the pure calcareous sediment suspension and the 3% $CaCO_3$ suspension.

The standard error of the blank over the 60 s acquisition period (5.85×10^{-8}–1.40×10^{-7}) was roughly the same as observed in the 1-cm path length analyses. Consistent with the observed 10-fold increase in sensitivity, this corresponds to an

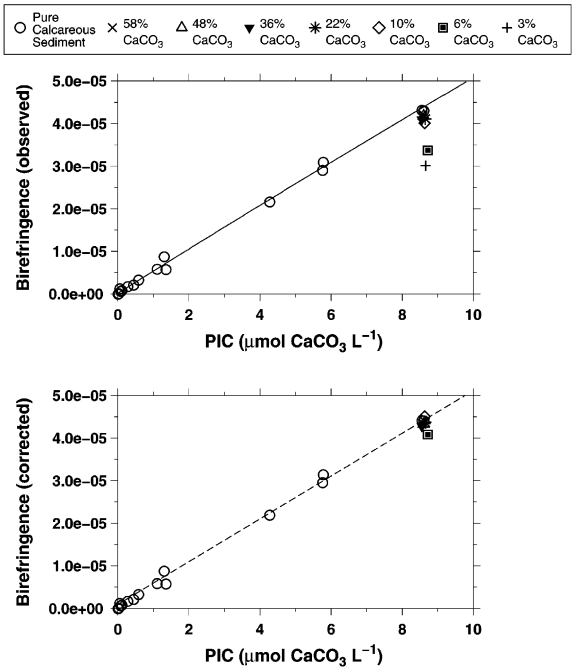

Fig. 9. (a) Observed and (b) corrected birefringence at 660 nm (10-cm path length) for the pure calcareous sediment samples and the mixed suspensions containing both calcareous sediment and diatomaceous earth. The solid line on the upper graph indicates the least-squares polynomial regression (order = 2) of observed birefringence on PIC for all pure calcareous sediment samples. The dashed line on the lower graph indicates the least-squares linear regression of corrected birefringence on PIC for the combined data from all of the samples containing calcareous sediment (3–100% $CaCO_3$, by weight).

instrumental detection limit of 0.04–0.08 μmol $CaCO_3 l^{-1}$ (i.e., an order of magnitude lower than that observed for the 1-cm path length analyses). The standard error for the samples (4.66×10^{-8} to 5.61×10^{-7}) covered roughly the same range as observed in the 1-cm analyses and was also generally greater for the samples with highest concentrations of $CaCO_3$.

The standard deviation of the triplicate analyses of the 0.12, 10.3, 11.5, and 49.6 μmol $CaCO_3 l^{-1}$ samples ranged from 3.32×10^{-7} to 4.37×10^{-6}. In each case, the standard deviation of the triplicate analyses was roughly an order of magnitude higher than the standard error of the birefringence signal over the 60 s acquisition period for the individual sample analyses. It is therefore apparent that most of the uncertainty in the measurement is due to procedural error over this range of concentrations, and that the lowest PIC concentrations that can be practically measured will be above the instrumental detection limit defined by signal noise. This is confirmed by the 2σ error bars based on the triplicate analyses of the 0.12 μmol $CaCO_3 l^{-1}$ sample (Fig. 8a, inset), which nearly intersect the x-axis and indicate that PIC concentrations below ~ 0.1 μmol $CaCO_3 l^{-1}$ are analytically indistinguishable from zero at the 95% confidence level.

6. Discussion

The relationships observed between absorbance and TSM are consistent with Beer's law, which states that absorbance is linearly proportional to both optical path length and analyte concentration. In these experiments, absorbance is a measure of light attenuated from the incident beam due to both absorption and scattering by the particles suspended in the sample cell. The correlation between slope and $CaCO_3$ content (Fig. 5) is a result of the greater scattering efficiency of the $CaCO_3$ in the calcareous sediment relative to the amorphous SiO_2 in the diatomaceous earth.

When measuring birefringence, the instrument was configured to detect light from the incident beam that had lost its linear polarization because of interactions with birefringent material in the sample cell. Interactions with non-birefringent particles would result in scattering or absorption of the incident beam but would not be expected to change its polarization state in the forward direction—i.e., no light capable of reaching the detector would be produced. Our observations were consistent with these expectations: birefringence was detected in the pure and mixed suspensions containing calcareous sediment but not in the suspensions containing only diatomaceous earth (i.e., non-birefringent particles).

For the samples prepared from the pure calcareous sediment suspension, birefringence was linearly proportional to both the optical path length and PIC at low concentrations. The instrument response dropped, however, as total particle concentrations or the relative abundance of non-$CaCO_3$ particles in the samples increased (Figs. 6a, 7a, 8a and 9a). The observed decrease in sensitivity can be attributed to greater interference from scattering and absorption, which reduces the amount of incident light available to interact with birefringent material in the sample cell. In addition, a greater portion of the depolarized light produced by interactions between incident light and birefringent material in the cell becomes scattered or absorbed before it reaches the detector.

To account for the effects of scattering and absorption by particles, a corrected birefringence signal (B_{cor}) was calculated for each of the samples according to the following empirical relationship:

$$B_{cor} = B_{obs}/T^{k}, \tag{3}$$

where B_{obs} is the observed birefringence signal for the sample, T is the non-polarized transmittance measured for the sample and k is an arbitrary constant. Samples having lower transmittance (indicating greater interference due to scattering and absorption) receive a larger upward correction to their birefringence signal. Best results were obtained with a k value of 0.5.

Applying this correction to the 1-cm path length results linearized the response curves for the suspensions with $CaCO_3$ content $\geqslant 9\%$ (Figs. 6b and 7b). Data for the pure calcareous sediment suspension and the mixed suspensions with $CaCO_3$ content between 32% and 64% converged toward

Table 4
Least-squares linear regressions of corrected birefringence (1-cm path length) on PIC for the pure calcareous sediment suspension and the mixed suspensions with $CaCO_3$ content between 9% and 64%. Two pure calcareous sediment samples with much higher PIC concentrations than the rest of the samples (1210 and 1820 μmol $CaCO_3\,l^{-1}$) were not included in these calculations

	Pure calcareous sediment	64% $CaCO_3$ mixed suspension	48% $CaCO_3$ mixed suspension	32% $CaCO_3$ mixed suspension	9% $CaCO_3$ mixed suspension	All suspensions ⩾32% $CaCO_3$
Number of samples	10	4	4	4	4	22
Slope ($l\,\mu mol^{-1}$)	6.03×10^{-7}	6.09×10^{-7}	6.22×10^{-7}	6.045×10^{-7}	3.99×10^{-7}	6.04×10^{-7}
Standard error	5.8×10^{-9}	1.8×10^{-8}	1.1×10^{-8}	9.1×10^{-8}	8.3×10^{-9}	5.4×10^{-9}
Intercept	-3.45×10^{-6}	-1.24×10^{-5}	-1.49×10^{-5}	-1.04×10^{-5}	-7.46×10^{-6}	-7.23×10^{-6}
Standard error	1.63×10^{-6}	6.54×10^{-6}	4.04×10^{-6}	3.26×10^{-6}	1.18×10^{-6}	1.78×10^{-6}
Correlation coefficient (r^2)	0.999	0.998	0.999	0.999	0.999	0.998

a single line (slope $= 6.04\times10^{-7}\,l\,\mu mol^{-1}$, Table 4). The slope for the 9% $CaCO_3$ suspension ($3.99\times10^{-7}\,l\,\mu mol^{-1}$) was approximately 34% lower than that of the more $CaCO_3$-rich suspensions. The correction scheme had little effect on the 3% $CaCO_3$ suspension data. For the 10-cm path length results, the corrected birefringence data for the pure calcareous sediment suspension and all of the mixed suspensions (3–58% $CaCO_3$ content) converged toward a single line (Figs. 8b and 9b). The slope ($5.03\times10^{-6}\,l\,\mu mol^{-1}$) was an order of magnitude higher than the slope of the line fit to the corrected 1-cm path length data for suspensions with $CaCO_3$ content ⩾9%. These results, which cover a range of PIC concentrations and PIC:TSM proportions characteristic of much of the surface ocean, show that conventional transmittance measurements can be used to correct the birefringence signal for interference due to scattering and absorption.

7. Conclusions

To our knowledge, this work is the first instance of using birefringence measurements to quantify PIC. Using a benchtop spectrophotometer equipped with linear polarizers, we have demonstrated a positive relationship between birefringence and PIC up to concentrations roughly 15 times greater than the highest values recorded in marine waters. Although PIC concentrations characteristic of open ocean, sub-euphotic zone waters lie below the detection limit, much of the range of PIC typically encountered in surface ocean waters is encompassed by the analytical range of the instrument equipped with a 10-cm cell. Based on the observed linear relationship between the sensitivity and path length, increasing the path length to 25 cm (a standard path length for marine transmissometers) would be expected to further reduce the detection limit by a factor of 2.5. Conventional (i.e., non-polarized) transmittance measurements were used to correct the birefringence signal for the sensitivity loss due to interference from scattering and absorption. At a path length of 10-cm, this correction scheme was successful for all of the samples containing calcareous sediment (3–100% $CaCO_3$ by weight).

Although the birefringence of organic marine particles was not directly assessed in these experiments, previous observations based on polarized light microscopy suggest that organic material is weakly birefringent relative to PIC. In addition, recent analyses performed at sea with the modified spectrophotometer detected no appreciable birefringence signal from particulate organic matter suspended in natural seawater samples (Guay and Bishop, unpublished data, 2001). Further insight will be gained from additional laboratory and field experiments investigating more complex particle suspensions having different size distributions and compositions (including living and detrital particulate organic matter as well as different classes of inorganic mineral particles).

Having thus established the proof-of-concept, we have built a prototype instrument based on a commercially available marine transmissometer for making in situ birefringence measurements of PIC in seawater. An in situ instrument with a path length of 10-cm or longer should be able to measure PIC concentrations down into the lower end of the oceanic range, provided that it was capable of equal or greater sensitivity and precision than the modified spectrophotometer. Note that in these experiments, the spectrophotometer was operated at a gain setting far above its normal operating range. In developing the in situ PIC sensor, the source lamp and detector electronics and other instrument parameters will be designed with the specific intent of obtaining the most stable birefringence signal over as much of the oceanic range of PIC as possible. Optimizing the performance of the in situ instrument will also reduce the required data acquisition period to enable continuous monitoring applications (e.g., water column profiling). A conventional transmissometer will be deployed simultaneously to allow correction of the birefringence signal and quantify particulate organic carbon (Bishop, 1999). In addition to standard ship-based deployment from a cable, the spatial dimensions and power requirements of the in situ PIC sensor are appropriate for long-term deployment on autonomous oceanographic platforms, including the SOLO profiling float (Sherman and Davis, 1995) and the self-navigating submarine glider *Spray* (Sherman et al., in press).

Acknowledgements

This work was supported by the National Oceanographic Partnership Program (ONR N00014-99-F450), the US Department of Energy Office of Science (grant KP120203), and the NOAA Postdoctoral Program in Climate and Global Change (administered by the University Corporation for Atmospheric Research). Samples of marine sediment material were obtained from B. Conard and N. Pisias at the Oregon State University Core Laboratory (supported by NSF grant OCE97-12024). A. Simmons, J. Wan and G. Waychunas provided access to their laboratory facilities at LBNL. Technical assistance was provided by T. Wood and L. Hsu. Valuable comments and discussion were contributed by R. Collier, J. Dymond, A. Hunt, G. Klinkhammer, G. Waychunas and two anonymous reviewers. This is LBNL Publication 46895.

References

Balch, W.M., Kilpatrick, K.A., 1996. Calcification rates in the equatorial pacific along 140°W. Deep-Sea Research II 43 (4–6), 971–993.

Balch, W.M., Kilpatrick, K.A., Trees, C.C., 1996a. The 1991 coccolithophore bloom in the central North Atlantic, I. Optical properties and factors affecting their distribution. Limnology and Oceanography 41 (8), 1669–1683.

Balch, W.M., Kilpatrick, K.A., Holligan, P., Harbour, D., Fernandez, E., 1996b. The 1991 coccolithophore bloom in the central North Atlantic, II. Relating optics to coccolith concentration. Limnology and Oceanography 41 (8), 1684–1696.

Berge, G., 1962. Discoloration of the sea due to *Coccolithus Huxleyi* "bloom". Sarsia 6, 27–40.

Bishop, J.K.B., 1989. Regional extremes in particulate matter composition and flux: effects on the chemistry of the ocean interior. In: Berger, W.H., Smetacek, V.S., Wefer, G. (Eds.), Productivity of the Ocean: Present and Past. Wiley, New York, pp. 117–137.

Bishop, J.K.B., 1999. Transmissometer measurement of POC. Deep-Sea Research I 46, 353–369.

Bishop, J.K.B., Ketten, D., Edmond, J.E., 1978. The chemistry, biology and vertical flux of particulate matter from the upper 400 m of the cape basin in the southeast Atlantic Ocean. Deep-Sea Research 25, 1121–1161.

Bishop, J.K.B., Wood, T.J., Mudge, T.D., 1998. Continental margin iron inputs and North Pacific bloomlets: Results from MULVFS deployments during CJGOFS cruises. Eos, Transactions, American Geophysical Union, Vol. 79, OS32I-05.

Brown, C.W., Yoder, J.A., 1994. Coccolithophorid blooms in the global ocean. Journal of Geophysical Research 99 (C4), 7467–7482.

Holligan, P.M., Fernandez, E., Aiken, J., Balch, W.M., Boyd, P., Burkill, P.H., Finch, M., Groom, S.B., Malin, G., Muller, K., Purdie, D.A., Robinson, C., Trees, C.C., Turner, S.M., van der Waal, P., 1993. A biogeochemical study of the coccolithophore, *Emiliania Huxleyi*, in the North Atlantic. Global Biogeochemical Cycles 7 (4), 879–900.

Macklin, S.A. (Ed.), 1999. Report on the FOCI international workshop on recent conditions in the Bering Sea, NOAA/PMEL, Publication No. B358-P-0, Seattle, Washington, 47pp.

Milliman, J.D., Troy, P.J., Balch, W.M., Adams, A.K., Li, Y.H., Mackenzie, F.T., 1999. Biologically mediated dissolution of calcium carbonate above the chemical lysocline. Deep-Sea Research I 46, 1653–1669.

Neese, W.D., 1991. Introduction to Optical Mineralogy. Oxford University Press, New York, 335pp.

Rossi, B.B., 1957. Optics. Addison-Wesley Publishing Company, Reading, MA, 510pp.

Sherman, J.T., Davis, R.E., 1995. Observations of temperature microstructure in NATRE. Journal of Physical Oceanography 25, 1913–1929.

Sherman, J.T., Davis, R.E., Owens, W.B., Valdes, J., The autonomous underwater glider 'Spray'. IEEE Journal of Oceanic Engineering, in press.

Tyrell, T., Holligan, P.M., Mobley, C.D., 1999. Optical impacts of oceanic coccolithophore blooms. Journal of Geophysical Research 104 (C2), 3223–3241.